Walisongo Journal of Chemistry
Walisongo Journal of Chemistry Vol. 8 Issue 1 (2025), 74-86
ISSN: 2621-5985 (online); 2549-385X (print)
DOI: https://doi.org/10.21580/wjc.v8i1.25794

REDOX AND THERMODYNAMIC INVESTIGATION OF 2-HYDROXYETHYLETHYLENEDIAMINETRIACETATOIRON(III) REACTION WITH 2-MERCAPTOETHANOLIC ACID IN A BICARBONATE-BUFFERED ENVIRONMENT

Ikechukwu Ugbaga Nkole[1*] , Sulaiman Ola Idris[2] , Ameh David Onu[3]

[1]Wigwe University, Nigeria
[2]Ahmadu Bello University, Nigeria
[3]Nigeria Federal University of Education Zaria, Nigeria

*Corresponding author: nkoleikechukwu@gmail.com

Abstract

The coordination chemistry of hexadentate ligands is compelling, as it provides both kinetic and thermodynamic stability to the coordinated complex, facilitating electron distribution while preserving structural integrity. In this study, the redox behavior of the reaction between 2-hydroxyethylethylenediaminetriacetatoiron(III) (HEI) and 2-mercaptoethanolic acid (MEA) was investigated spectrophotometrically in a bicarbonate-buffered environment. The reaction followed first-order kinetics with respect to [HEI] and [MEA], with a 2:2 molar ratio observed. The reaction rate was significantly affected by increases in the ionic strength and the dielectric constant of the medium. Ion catalysis was evident, and variations in pH had a significant effect on the redox pathway. Activation enthalpy and Gibbs free energy, as determined via the Eyring–Polanyi equation, indicate that the reaction required additional thermal energy to proceed. The formation of thiyl radicals facilitated the conversion of the mercapto compound to a disulfide. A Michaelis-Menten-type plot (MMTP) supported the absence of intermediate species participation, as indicated by a negative result, further corroborated by matching spectroscopic spectra of reacted and unreacted mixtures. The proposed mechanism offers insight into the potential anticancer activity of mercaptoethanolic acid.

Keywords: *2-mercaptoethanolic acid, Hexadentate ligand, pH, Redox, Thermodynamic*

Introduction

The coordination chemistry of bioinorganic moieties has attracted significant interest over the years due to their critical importance in addressing diseases, enhancing drug potency, and designing sustainable chemical and biochemical feeds (Dennis et al., 2021; Nkole et al., 2022; Sar & Saha, 2020). Iron-containing coordinated moieties, in particular, are not overlooked, as iron is one of the key players in biological coordination, typically forming oxo- or hydroxo-bridged, as well as di- or polynuclear frameworks (Haas et al., 2009). Several dinuclear iron(III) enzymes, such as ferritin for iron storage and hemerythrin for oxygen transfer, play vital roles in biological systems (Rodgers et al., 2019).

Polyaminecarboxylate chelates have extensive applications in coordination chemistry, with well-documented uses in analytical and environmental chemistry

(Zhang et al., 2023). These applications include effluent isolation, bioremediation of contaminants, chemical catalysis, and the assembly of supramolecules. The structures of Fe(III) complexes with polyamine carboxylates are particularly intriguing because they can adopt six- and seven-coordination due to the critical radius of the Fe(III) cation (0.79 Å) and the spherically symmetrical high-spin d^5 electronic configuration of the metal ion. Several structures of Fe(III) and Fe(II) complexes have been reported in which the hexadentate ligand is bound to a single iron center, forming an octahedral coordination at the seventh position (Kelly et al., 2022).

On the other hand, tetradentate salen-ligands have been coordinated with iron(III), and their redox behavior with oxalic acid has been studied in a mixture of water and dimethyl sulfoxide. It was observed that charge distribution and acid concentration variation in the medium inhibited the redox progress. The kinetic order of the redox partner was first order in each partner, and the contribution of intermediate species was not feasible. The coordinated salen-Fe^{3+} complex maintained its structural integrity, with an electron differential of 2+ in the coordinated product. In contrast, the oxalic acid was broken down into CO_2 and H_2O in a 2:3 (salen-Fe^{3+}: oxalic) stoichiometry, and the overall rate of the redox process was $7.29 \pm 0.2 \times 10^{-1} M^{-1} s^{-1}$ (Ibrahim et al., 2019). Additionally, octahedral-coordinated Schiff-base-iron(III) moieties have been reported to destroy both gram-positive bacteria (*P. aeruginosa* and *S. pyogenes*) and gram-negative bacteria (*E. coli*). Due to the charge distribution between Fe^{3+} and the ligands, the ability of the coordinated moieties to solubilize in the cell lipid membrane facilitates their direct bombardment of bacteria via redox processes (Abu-Dief et al., 2015).

The reduction potential of thiol-containing biomolecules is typically pH-dependent, with the deprotonated form of every thiol affected by the solution's pH, usually in the range of 6-11 (Rippel, 2012). The mechanistic study of the redox reactions of sulfur-containing moieties and their derivatives has attracted significant attention in chemistry and biochemistry research, as these systems serve as models for the corresponding redox processes in biological systems (Hand et al., 2005).

However, 2-mercaptoethanolic acid possesses two transferable electrons from its mercapto (sulfur) group and carboxyl group, forming adducts with esters, amides, and anilides (Chakraborty et al., 2013). A mild procedure for the trapping of lignin has been reported to be facilitated by the use of 2-mercaptoethanolic acid in combination with boron trifluoride (Rippel, 2012). Oxidation of 2-mercaptoethanolic acid with nickel(III)-oxime-imine (Dutta et al., 1997), dinuclear molybdenum complexes (Demirhan et al., 2006), hexaaquoiron(III) ions (Ellis et al., 1975), and EDTA-Mn^{3+} complexes (Gangopahyay et al., 1994) has been reported. Therefore, the researchers aimed to explore its redox transformation in a biochemical system involving hexadentate-ligand-Fe^{3+} coordination within a controlled pH environment in greater depth. Furthermore, the researchers anticipate that the kinetic data generated can provide further insight into the pace of anti-cancer activity of thiols on tumors while also exploring the thermodynamic aspects. The kinetic data obtained is expected to contribute additional information on the rate dynamics of the iron-ligand framework in interaction with thiols.

Methodology

Materials

Iron(III) nitrate, 2-hydroxyethyl-ethylenediaminetriacetatic acid (HEDTA), sodium bicarbonate, 2-mercaptoethanolic acid (MEA), sodium carbonate, potassium nitrate, acetone, sodium sulfate, ammonium nitrate, acrylamide, methanol, and diethyl ether were supplied by Fluka Chemicals.

Synthesis

The2-hydroxyethylethylenediamine - triacetatoiron(III) (HEI) was prepared following the approach of Xiao-juan (Mirbolook et al., 2023) and characterized

using a UV-Visible spectrometer (Cary 300 Series, Agilent Technologies) and FTIR (FTIR-8400S Shimadzu).

A 40 cm^3 solution of 3.36 g of HEDTA was stirred, and a 40 cm^3 solution of 2.42 g of $Fe(NO_3)_3$ was added dropwise. The mixture was made up of distilled water to 100 cm^3 and stirred for 4 hours with a magnetic stirrer. A light brown crystal was obtained after immersing the mixture in an ice bath and washing it with cold distilled water. The initial pH of 3.7 of the HEI solution was adjusted to 7.5 with a bicarbonate-buffer solution. The HEI was stored in an amber-colored bottle in a dark cupboard (Mirbolook et al., 2023).

Stoichiometry and product analysis

The spectrophotometric mole ratio procedure was employed (Arthur et al., 2024; Nkole et al., 2024; Umoru et al., 2024), and it was achieved by recording the absorbance of reaction solutions in the range (0.2 - 1.8) × 10^{-3} M (MEA), with constant [HEI], μ = 0.9 M (KNO_3), pH = 7.5 (bicarbonate buffer), and temperature = 301 K. A Corning Colorimeter 252 at 490 nm was used to record the absorbance of the mixtures until the absorbance remained unchanged. A point of inflection on the curve of the relationship between absorbance and mole ratio corresponds to the stoichiometry of the redox reaction.

An extraction analysis that identifies the presence of a disulfide product was performed following the reported procedure (Ibrahim et al., 2022; Nkole et al., 2021; Osunkwo et al., 2018). The product mixture was extracted six times with diethyl ether, and the ether layer was washed in batches with diethyl ether and left to dry in a desiccator. The aqueous layer was scanned with a UV-Visible spectrometer to trace the presence of Fe^{2+} ions (Comini, 2016).

Kinetic analysis

The redox rate was investigated by deploying a pseudo-first-order condition in the concentration of the redox species and monitoring the change in the absorbance of [HEI] at 490 nm on a Sherwood Colorimeter 254 while the pH, ionic strength, and temperature were kept constant (Abdulsalam et al., 2020; Geidaroy et al., 2023; Nkole et al., 2022; Nkole et al., 2022; Oladunni et al., 2020; Quinones et al., 2024). The relationship between log (A_t - A_∞) and time was analyzed following the kinetic equations (Equations i, ii, and 1), and the slope of the graph was used to calculate the observed rate constant (k_0). The second-order rate constant (k_2) was determined from the ratio of k_0 to [MEA]. The effects of pH, ionic strength (μ), and dielectric constant (D) on the rate were investigated with pH values ranging from 6 to 10, ionic strengths from 0.3 to 1.0 M, and dielectric constants from 80.1 to 62.2 (acetone input), while all other parameters were kept constant.

$$A_t = A_0 e^{-kt} \quad \text{(i)}$$

$$\ln A_t = \ln A_0 - kt \quad \text{(ii)}$$

$$\log(A_t - A_{\infty)}) = -kt \quad (1)$$

The effect of counter-ions Y (Y = SO_4^{2-} and NH_4^+) on the redox mixture was examined for [Y] = (1.0 – 21.0) × 10^{-3} M, while the conditions of all other species were kept unchanged (Han et al., 2020; Myek et al., 2020; Nkole et al., 2021; Nkole et al., 2022; Shanmugaprabha et al., 2016).

The activation of free radicals in the process was investigated by adding a 5 cm^3 (0.28 M) acrylamide solution to the ongoing redox mixture, followed by adding excess methanol. A control experiment was conducted by adding the same amount of acrylamide solution and methanol to a separate solution of HEI and MEA (Nkole et al., 2021; Nkole et al., 2023; Ukoha et al., 2015). Kinetic evidence, including a Michaelis-Menten-type plot (MMTP) and spectroscopic scan, were used to ascertain the involvement of intermediate species in the reaction (Asghar & Fawzy, 2016; Osunkwo et al., 2018).

The effect of redox temperature on the redox rate was investigated by varying the temperature (301-341 K). The thermodynamic parameters of the redox medium were estimated using the Eyring-Polanyi plot (EPP), $\ln(\frac{k_2}{T})$ against $\frac{1}{T}$, where the activation enthalpy ($\Delta H^{\ddagger}$) was derived from the slope, the activation entropy ($\Delta S^{\ddagger}$)

Copyright © 2025 WJC | ISSN 2621-5985 (online) | ISSN 2549-385X (print)
Volume 8, Nomor 1, 2025

from the intercept, and the Gibbs free energy ($\Delta G^{\ddagger}$) from the following equation (2):

$$\Delta G^{\ddagger} = \Delta H^{\ddagger} - T\Delta S^{\ddagger} \quad (2)$$

The EPP equation (3) is given as follows (Nkole et al., 2022; Srinivasan, 2022):

$$\ln\left(\frac{k_2}{T}\right) = \ln\left(\frac{K_b}{h}\right) + \frac{\Delta S^{\ddagger}}{R} - \frac{\Delta H^{\ddagger}}{RT} \quad (3)$$

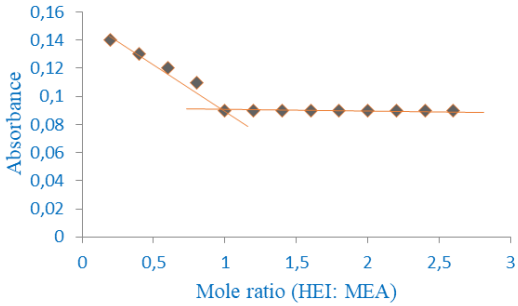

Figure 1. Stoichiometric relationship between HEI and MEA Condition: [HEI] = 9.7 × 10-3 M, μ = 0.9 M, [MEA] = (1.94 – 25.22) × 10-3 M, pH = 7.5, max. abs. = 490 nm, and T = 301

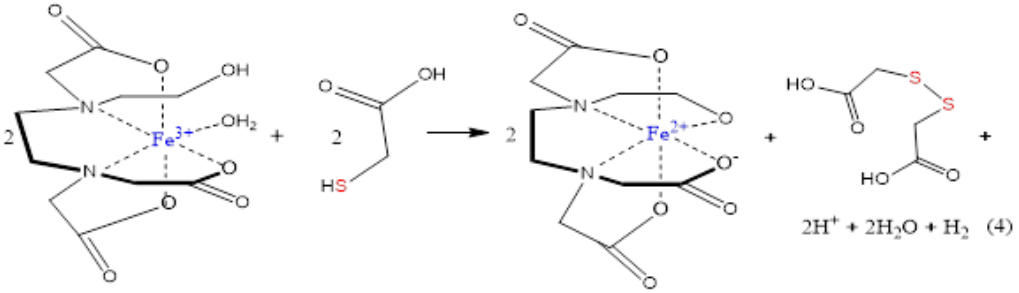

Results and Discussion

Characterization of the HEI

The UV-Visible spectrometer and FTIR were used to obtain the maximum absorption and confirm the bond formation between HEDTA and the iron metal center, respectively. The UV-Visible spectrum of the HEI showed maximum absorption at 368 and 490 nm. The FTIR spectra of the HEDTA and HEI showed bands at 1273.06 cm^{-1} (C-N), 1620.26 cm^{-1} (C=O); and 601.81 cm^{-1} (Fe-N), 848.71 cm^{-1} (Fe-O), respectively. The observed peak at 490 nm from the UV-Visible scan was used to monitor the reaction, and the bands from the FTIR spectra validated the bond formation between the metal center and the electron pair donors (O and N) of the HEI.

Stoichiometry

As presented in Figure 1, the stoichiometric study showed that an equal mole ratio of HEI and MEA was required to form the product species, as underpinned by Equation 4.

The appearance of crystals after extracting the product mixture with diethyl ether suggests thiyl disulfide as a component of the product. This finding aligns with the study by Abdulsalam et al. (2023) on thiols. The maximum peak at 520 nm (see Figure 2) suggests the presence of the Fe^{2+} moiety, as reported by Comini (2016).

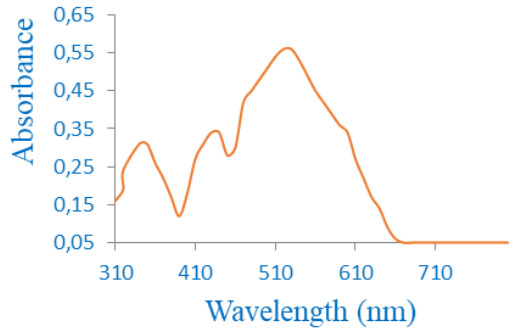

Figure 2. UV-Visible spectrum of the HEI-MEA product

Table 1. Redox-rate constants of the reaction Condition: [HEI] = 9.7 × 10-3 M, μ = 0.9 M, pH = 7.5, D = 80.1, T = 301 K, and max. abs. = 490 nm.

10^2[MEA], M	pH	μ, M M^{-1} s^{-1}	10^3k_0, s^{-1}	10^2k_2,
1.0	7.5	0.90	0.87	8.87
2.0	7.5	0.90	1.77	8.86
3.0	7.5	0.90	2.63	8.75
4.0	7.5	0.90	3.39	8.46
5.0	7.5	0.90	3.52	8.19
6.0	7.5	0.90	4.55	8.25
7.0	7.5	0.90	6.24	8.91
8.0	7.5	0.90	6.79	8.49

The pseudo-first-order plot was linear (see Figure 3), and a slope of 0.9806 was obtained from the relationship between log k_0 and log [MEA] (see Figure 4). The linearity in Figure 3 and the slope of 0.9806 in Figure 4, approximating 1.0, indicate a first-order dependence on the concentration of HEI and MEA, as well as an overall second-order reaction. The values of k_0 and k_2 for the various concentrations of MEA are shown in Table 1. The relative uniformity of k_2 supports the first-order dependence on the concentration of MEA.

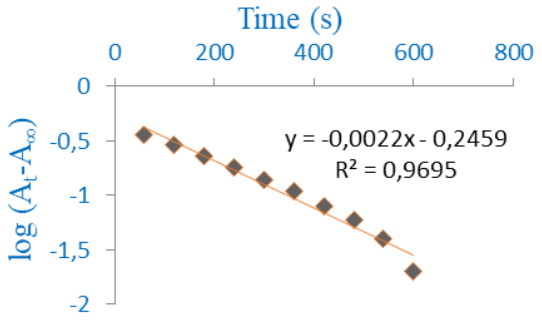

Figure 3. Classic pseudo-first-order plot for the reaction of HEI and MEA

The ionic strength of the redox medium affected the rate constant of the reaction by increasing it (see Table 2), suggesting that the core participating species in the redox process were like-charged ions, as supported by Equation 7. A plot of log k_2 against $\sqrt{\mu}$ (see Figure 5) gives a straight line with a slope of 1.074, indicating the magnitude of the charges on the redox species (Equation 7). This is further supported by the effect of changes in the medium's dielectric constant from 80.1 to 62.2 on the redox rate (see Table 3). The redox rate decreased as D decreased due to the reduction in the polarizing power of the redox mixture.

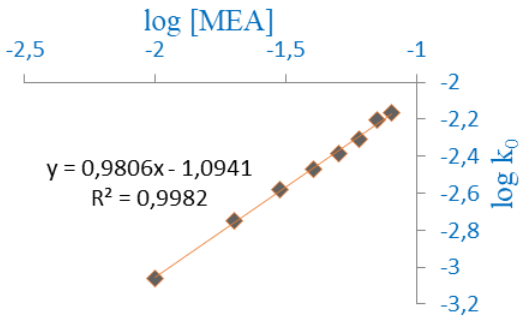

Figure 4. Logarithmic relationship between first-order rate constant and MEA concentration

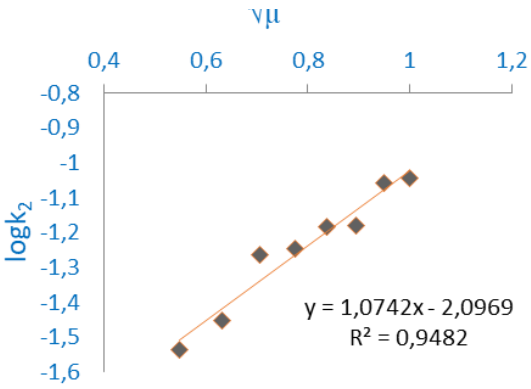

Figure 5. Relationship between log k2 and √μ for the reaction Condition: [HEI] = 9.7 × 10^{-3} M, [MEA] = 7.0 × 10^{-2} M, μ = (0.3 – 1.0) M, pH = 7.5, D = 80.1, T = 301 K, and max. abs. = 490 nm.

Table 2. Effect of ionic strength in the redox medium on the rate constant Condition: [HEI] = 9.7 × 10-3 M, μ = (0.3 – 1.0) M, pH = 7.5, D = 80.1, T = 301 K, and max. abs. = 490 nm.

μ, M	10^3k_0, s^{-1}	10^2k_2, M^{-1} s^{-1}
0.3	2.04	2.92
0.4	2.46	3.52
0.5	3.82	5.45
0.6	3.98	5.68
0.7	4.59	6.57
0.8	4.62	6.61
0.9	6.24	8.91
1.0	6.31	9.01

Table 3. Effect of the dielectric constant of the reaction medium on the rate constant Condition: [HEI] = 9.7 × 10-3 M, μ = 0.9 M, pH = 7.5, T = 301 K, and max. abs. = 490 nm

D	10^3k_1, s^{-1}	10^2k_2, M^{-1} s^{-1}
80.1	6.24	8.91
78.4	4.84	6.92
76.6	4.61	6.58
74.9	4.38	6.26
73.2	4.16	5.95
71.4	4.08	5.82
69.7	3.48	4.97
67.9	3.34	4.78
66.2	3.19	4.57

The result obtained from the pH-dependent study shows that changes in pH affected the redox rate, with a significant increase in the redox rate as the pH increased progressively. However, the rate dropped at neutral pH (see Figure 6). This favors the deprotonation of MEA and the dissociation of aqua molecules attached to the HEI. pH 10.0 is the most favorable pH for the fast reduction of the Fe^{3+}-complex (Gangopadhyay et al., 1994).

Adding monovalent ions (NH_4^+) to the redox medium accelerated the redox rate, while the opposite effect was observed for divalent ions (SO_4^{2-}). The effect exhibited by the added monovalent ion may be due to the increasing electric field produced by the monovalent ion, which orients the water molecules in such a way that their ability to adjust their orientations in the solvation shell of the ions becomes limited. Thus, electrostatic attraction and repulsion are implicated in the presence of monovalent ions and divalent ions, respectively. This observation supports a reaction proceeding via an outer-sphere mechanism, as proposed by Taube et al. (Abdulsalam et al., 2020; Myek et al., 2020).

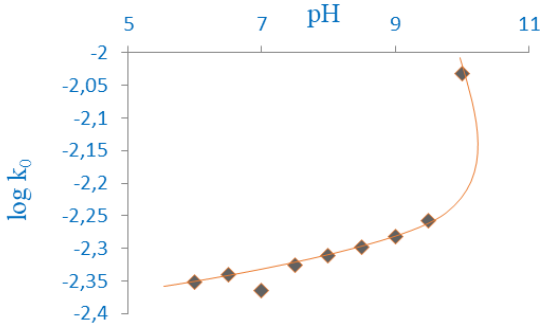

Figure 6. The curve of log k0 against pH Condition: [HEI] = 9.7 × 10-3 M, [MEA] = 7.0 × 10-2 M, μ = 0.9 M, pH = 6.0 – 10.0, D = 80.1, T = 301 K, and max. abs. = 490 nm.

Table 4. Effect of added monovalent and divalent ions to the redox medium on the rate constant condition: [HEI] = 9.7 × 10-3 M, μ = 0.9 M, pH = 7.5, D = 80.1, T = 301 K, and max. abs. = 490 nm.

ION	10^3[Ion], M	10^3 k_0, s^{-1}	10^2k_2, M^{-1} s^{-1}	ION	10^3[Ion], M	10^3k_0, s^{-1}	10^2k_2, M^{-1} s^{-1}
SO_4^{2-}	0.00	6.24	8.91	NH_4^+	0.00	6.24	8.91
	1.0	0.70	1.86		1.00	6.68	9.54
	3.0	0.78	1.11		3.00	7.10	10.14
	9.0	0.68	0.98		9.00	7.32	10.45
	12.0	0.67	0.96		12.0	7.53	10.75
	15.0	0.65	0.92		15.0	7.84	11.20
	18.0	0.64	0.91		18.0	8.21	11.20
	21.0	0.63	0.90		21.0	8.44	12.05

The generation of free radicals in the reaction is positive, as a gelatinous precipitate was observed on the acrylamide solution added to the partially reduced reaction mixture in excess methanol. This observation suggests the formation and utilization of free radicals during the anticancer action of MEA.

According to the Eyring-Polanyi equation, the relationship between $\ln\left(\frac{k_2}{T}\right)$ and $\frac{1}{T}$ gave a linear plot with an intercept at 2.946 and a gradient of -3568 (see Figure 7). Thus, the activation parameters ($\Delta S^{\ddagger}$ = -173.05 $Jmol^{-1}K^{-1}$ and $\Delta H^{\ddagger}$ = +29.66 $kJmol^{-1}$) corroborate the highly ordered nature of the transition-state species and the energy gain for its formation, respectively (Ibrahim et al., 2022). The feasibility of the reaction lies in the electron tunneling of the HEI through the metal ion to the nucleophilic-rich thiol, leading to the transformation of MEA into thiyl disulfide.

According to classical kinetics, an intermediate species was observed. Hence, the MMTP (see Figure 8) was linear with no intercept, indicating the absence of a bridging ligand in the redox species prior to electron transfer. The lack of a meaningful shift in the spectroscopic scan of the HEI and reaction mixture (see Figure 9) strengthened the MMTP. Moreover, the reaction was prone to ion catalysis, further supporting the results of the MMTP.

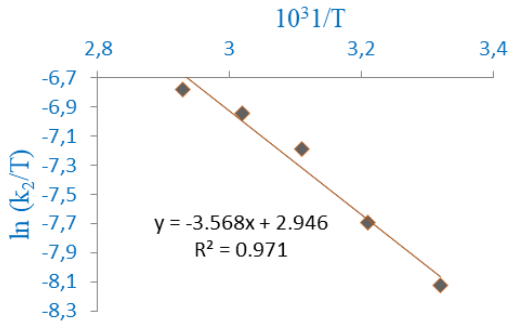

Figure 7. Relationship between ln⁡〖(k_2/T)〗 and 1/T for the reaction Condition: [HEI] = 9.7 × 10-3 M, [MEA] = 7.0 × 10-2 M, μ = 0.9 M, pH = 7.5, D = 80.1, T = (301 – 341) K, and max. abs. = 490 nm.

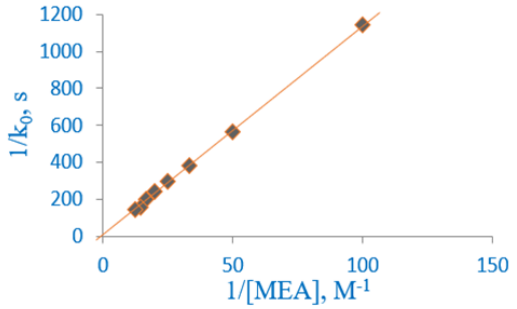

Figure 8. MMTP of 1/k0 against 1/[MEA] for the reaction Condition: [HEI] = 9.7 × 10-3 M, [MEA] = (0.01 – 0.08) M, μ = 0.9 M, pH = 7.5, D = 80.1, T = 301 K, and max. abs. = 490 nm.

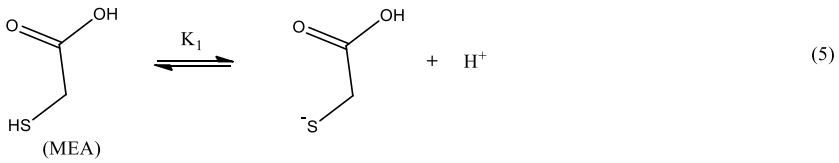

(5)

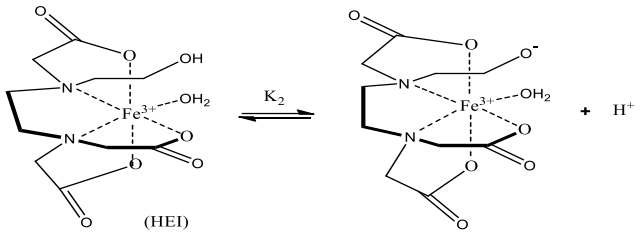

(6)

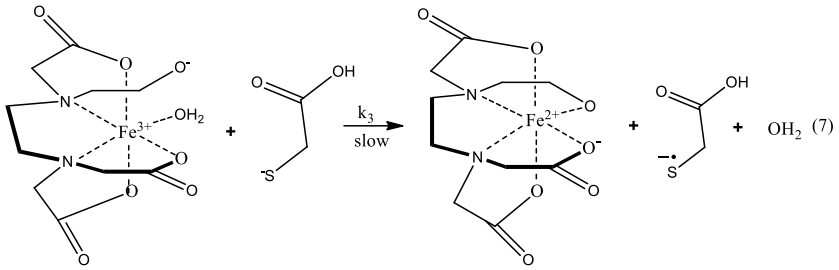

(7)

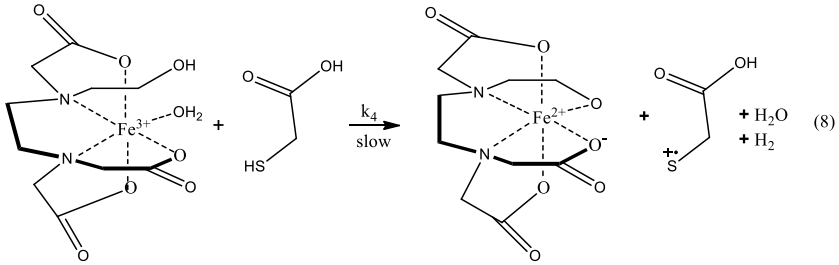

(8)

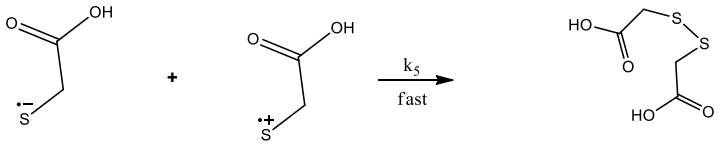

(9)

$$Rate = k_3[HEI^-][MEA^-] + k_4[HEI][MEA] \quad (10)$$

From Equations 5 and 6:

$$[MEA^-] = \frac{K_1[MEA]}{[H^+]} \quad (11)$$

$$[HEI^-] = \frac{K_2[HEI]}{[H^+]} \quad (12)$$

Substituting Equations 11 and 12 into Equations 10:

$$Rate = \frac{k_3K_1K_2[HEI][MEA]}{[H^+]^2} + k_4[HEI][MEA] \quad (13)$$

$$Rate = \frac{k_3K_1K_2 + k_4}{[H^+]^2}\ ([HEI][MEA]) \quad (14)$$

$$Rate = k[HEI][MEA] \quad (15)$$

where $k = \frac{k_3 K_1 K_2 + k_4}{[H^+]^2}$, and Equation 15 presents the reaction rate law. Thus, the above mechanism followed an outer-sphere pathway due to the kinetic evidence (the importance of ion catalysis and the absence of intermediate species formation) and spectroscopic evidence.

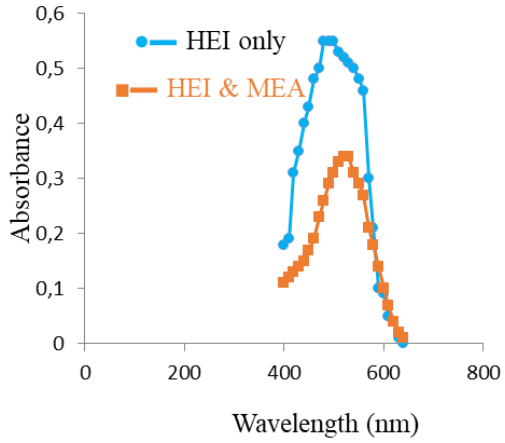

Figure 9. Spectroscopic scan of the reaction mixture

Conversely, the reaction of the Co(III)-salophen complex with 2-mercaptoethanolic acid in mixed solvent media exhibited first-order kinetics concerning the concentration of 2-mercaptoethanolic acid and Co(III)-salophen complex; two moles contributed from each reactant, resulting in the formation of dithiodiglycolic acid; free radical formation was not ruled out (Abdulsalam et al., 2023).

A mechanism incorporating ion catalysis, an MMTP intercept-free pathway, deprotonation, ionic strength, free radical liberation, and the absence of intermediate species was proposed (Equations 5–9). The mechanism involved the deprotonation of MEA and HEI (Equations 5 and 6), the collision of the deprotonated species with a similar charge serving as the first rate-determining step (Equation 7), and the collision of unprotonated species serving as the second rate-determining step (Equation 8), depicting a reaction with two pathways, where the first rate-determining step is the major slow step, which reflects the ionic strength, dielectric constant, and ion catalysis observations. The fast propagation of the thiyl radicals generated from the two rate-determining steps gave the disulfide (Equation 9). Thus, the redox rate law was derived from this (Equations 10–15).

Conclusion

The redox and thermodynamic investigation of 2-hydroxyethylethylenediaminetriacetatoiron (III) in a buffer-sensitive environment with 2-mercaptoethanolic acid was conducted. The process followed a 2:2 stoichiometry with a reaction exhibiting first-order kinetics in both [HEI] and [MEA]. There was a progressive increase in the reaction rate as the pH approached alkalinity. The reaction was sensitive to changes in the ionic strength of the medium, indicating the composition of transition-state species by like-charged redox species. A stable intermediate species was ruled out, and free-radical intervention was evident. The maintenance of the iron complex's structural integrity suggests the molecule's sustainability in the progressive redox cycle. Evidence from the study indicates that the reaction proceeded via the outer-sphere mechanism, providing further insight into the rate and pathways of thiols in relation to their breakdown in cancer cells.

References

Abdulsalam, S., Idris, S. O., Shallangwa, G. A. & Onu, A. D. (2023). Oxidation of thioglycolic acid by Co(III) salophen in binary mixed DMSO-Water and sodium dodecyl sulfate media. Chemistry Africa, 7(2), 1011-1019.

https://doi.org/10.1007/s42250-023-00786-1

Abdulsalam, S., Idris, S. O., Shallangwa, G. A. & Onu, A. D. 2020. Reaction of N, N1-phenylenebis(salicylideneiminato)cobalt(III) and l-cysteine in mixed aqueous medium: kinetics and mechanism. Heliyon, 6, e04621. https://doi.org/10.1016/j.heliyon.2020.e03850

Abu-Dief, A. M. & Mohamed, I. M. A. (2015). A review on versatile applications of transition metal complexes incorperating Schiif bases. Beni-Suef Univeristy Journal of Basic Applied Sciences, 4, 119-133. https://doi.org/10.1016/j.bjbas.2015.05.004

Arthur, D. E., Nkole, I. U. & Osunkwo, C. R. (2024). Electron transfer reaction of tris-(1,10-phenanthroline)cobalt(III) complex and iodide ion in an aqueous acidic medium. Chemistry Africa, 4, 63-69. https://doi.org/10.1007/s42250-020-00201-z

Asghar, H. & Fawzy, A. (2016). Kinetic, mechanistic, and spectroscopic studies of permanganate oxidation of azinylformamidines in acidic medium, with autocatalytic behavior of manganese(II). Journal of Saudi Chemical Society, 20, 561-569. https://doi.org/10.1016/j.jscs.2014.12.001

Chakraborty, M., Mandal, P. C. & Mukhopadhyay, S. (2013). Kinetic studies on oxidation of l-cysteine and 2-mercaptoethanol by trinuclear Mn(IV) species in aqueous acidic media. Inorganica Chimica Acta, 398, 77-82. https://doi.org/10.1016/j.ica.2012.12.015

Comini, M. A. (2016). Measurement and meaning of cellular thiol: disulphide redox status. Free Radical Research, 50(2), 246-271. https://doi.org/10.3109/10715762.2015.1110241

Demirhan, F., Taban, G., Baya, M., Dinoi, C., Daran, J. & Poli, R. (2006). Reduction of [Cp*2Mo2O5] by thioglycolic acid in an aqueous medium: synthesis and structure of [{Cp*Mo(μ-SCH2COO)}2(μ-5)]. Journal of Organometallic Chemistry, 691, 648-654. https://doi.org/10.1016/j.jorganchem.2005.10.006

Dennis, C. R., Van Zyl, G. J., Fourie, E., Basson, S. S. & Swarts, J. C. (2021). A kinetic study of the oxidation of the tetrakisoxalatouranate(IV) ion by the hexacyanoferrate(III) ion in an oxalate buffer medium. Reaction Kinetics Mechanisms and Catalysis, 132, 599-615. https://doi.org/10.1007/s11144-021-02109-2

Dutta, A., Basudeb, S., Mohammad, A. & Pradyot, B. (1997). Kinetics of oxidation of thioglycolic and thiomalic acids by a nickel(III) oxime-imine complex. Journal of Chemical Research (S), 186-187.

Ellis, K. J., Lappin, A. G. & McAuley, A. (1975). Metal ion oxidations in solution. part xv. rate determining dimerisation in redox reactions of iron(III) with some mercaptocarboxylic acids. Journal of Chemical Society Dalton Transaction, 0, 1930-1934.

Gangopahyay, S., Ali, M., Dutta, A. & Banerjee, P. (1994). Oxidation of thioglycolic acid and glutathione by (trans-cyclohexane-1,2-diamine-N, N, N1, N1-tetraacetato)manganese(III) in aqueous media. Journal of American Chemical Society Dalton Transactions, 3, 841-845. https://doi.org/10.1039/DT9940000841

Geidarov, A. A., Abbasova N. I. Dzhabbarova, Z. A., Ibragimova, A. A. & Alyshanly, G. I. (2023). Kinetics and thermodynamics of iron(III) ion removal from aqueous solution by Dowex G-26(H) resin. Russian Metallurgy, 2023, 1665-1671. https://doi.org/10.1134/S0036029523110071

Haas, K. L. & Franz, K. J. (2009). Application of metal coordination of chemistry to explore and manipulate cell biology. Chemical Reviews, 109(10), 4921-4960. https://doi.org/10.1021/cr900134a

Han, J., Lu, Z., Hammond, G. B. & Xu, B. (2020). Transition-State expansion: a quantitative model for counterion effects in ionic reactions. iScience, 23(10), 101593. https://doi.org/10.1016/j.isci.2020.101593

Hand, C. E. & Honek, J. F. (2005). Biological chemistry of naturally occurring thiols of microbial and marine origin. Journal of Natural Products, 68(2), 293-238. https://doi.org/10.1021/np049685x

Ibrahim, I., Idris, S. O., Abdulkadir, I. & Onu, A. D. (2019). Kinetics and mechanism of the redox reaction of N,N′-phenylenebis-(salicylideneiminato)iron(III) with oxalic acid in mixed aqueous medium. Transition Metal Chemistry, 44(3), 269-273. https://doi.org/10.1007/s11243-018-0291-8

Ibrahim, I., Idris, S. O., Abdulkadir, I. & Onu, A. D. (2022). Thioglycolic acid oxidation by N, N'-phenylenebis(salicylideneiminato)manganese(III) in DMSO/H2O: effects of sodium dodecyl sulfate and cetyltrimethylammonium bromide. Results in Chemistry, 4, 100541. https://doi.org/10.1016/j.rechem.2022.100541

Kelly, C. T., Griffin, M., Esien, K., Felton, S., Muller-Bunz, H. & Morgan, G. G. (2022). Crystallographic detection of the spin state in Fe(III) complexes. Crystal Growth and Design, 22, 6429-6439. https://doi.org/10.1021/acs.cgd.2c00468

Mirbolook, A., Alikhani, M., Sadeghi, J. & Lakzian, A. (2023). Synthesis and characterisation of Schiff base Fe(II) complex as a new iron source in nutrient solution. Rhizosphere, 25, 100664. https://doi.org/10.1016/j.rhisph.2023.100664

Myek, B., Idris, S. O., Onu, A. D. & Yakubu, M.K. (2020). Kinetics and mechanism of the redox reaction of Orange II with thiosulphate ion in aqueous acid. Science World Journal, 15, 108-111.

Nkole, I. U., Abdulsalam, S., Ibrahim, I. & Arthur, D. E. (2021). Micellar effect on electron transfer reaction of 2-(hydroxyethyl)ethylenediaminetriacetatoiron(III) complex with thiocarbonate ion: kinetic model. Chemistry Africa, 4, 525-533. https://doi.org/10.1007/s42250-021-00241-z

Nkole, I. U., Idris, S. O., Abdulkadir, I. & Onu, A. D. (2022). Application of Piszkiewicz model on the electron transfer reaction of dithionite ion and bis-(2-pyridinealdoximato)dioxomolybdate(IV) complex. Scientific Reports, 12, 22125. https://doi.org/10.1038/s41598-022-24096-7

Nkole, I. U., Idris, S. O., Abdulkadir, I. & Onu, A. D. (2022). Effect of surfactant micellization on the oxidation of mercaptobenzothiazole by bioinorganic molybdenum complex. Results in Chemistry, 2, 100616. https://doi.org/10.1016/j.rechem.2022.100616

Nkole, I. U., Idris, S. O., Abdulkadir, I. & Onu, A. D. (2022). Redox reaction of bis-(2-pyridinealdoximato)dioxomolybdate(IV) complex with thiosulphate Ion in aqueous acidic and surfactant media. Inorganic Chemistry Communications, 140, 109468. https://doi.org/10.1016/j.inoche.2022.109468

Nkole, I. U., Idris, S. O., Abdulkadir, I. & Onu, A. D. (2022). The study of redox reaction of gallic acid with bis-(2-pyridinealdoximato)dioxomolybdate(IV) complex in an aqueous acidic medium. Chemistry Africa, 5, 525-532. https://doi.org/10.1007/s42250-022-00346-z

Nkole, I. U., Idris, S. O., Abdulkadir, I. & Onu, A. D. (2023). Cationic surfactant-based catalysis on the oxidation of glutamic acid by bis-(2-pyridinealdoximato)dioxomolydate(IV) complex. Catalysis Letters, 153(12), 1-10. https://doi.org/10.1007/s10562-022-04187-w

Nkole, I. U., Idris, S. O., Abdulkadir, I. & Onu, A. D. (2024). Oxidation of aspartic acid with molybdenum-oxime-ligand framework in acidified-aqua and interfacial active media: Menger-Portnoy kinetic model. Inorganic Chemistry Communications, 161, 111979. https://doi.org/10.1016/j.inoche.2023.111979

Nkole, I. U., Idris, S. O. & Onu, A. D. (2021). Redox reactions of tris-(1,10-phenanthroline)iron(III) complex with thiourea and N-methylthiourea in aqueous acidic medium: kinetics and mechanism. Inorganic Chemistry Communications, 133, 108930. https://doi.org/10.1016/j.inoche.2021.108930

Nkole, I. U., Idris, S. O., Onu, A. D. & Abdulkadir, I. (2022). The study of Piszkiewicz's and Berezin's models on the redox reaction of allylthiourea and bis-(2-pyridinealdoximato)dioxomolybdate(IV) complex in an aqueous acidic medium. Beni-Suef University Journal of Basic Applied Sciences, 11, 68. https://doi.org/10.1186/s43088-022-00249-5

Nkole, I. U. & Idris, S. O. (2021). Thermodynamics and kinetic investigation of reaction of acriflavine with l-cysteine in aqueous medium. Chemistry Africa, 4, 731-740. https://doi.org/10.1007/s42250-021-00280-6

Oladunni, N., Idris, S. O. & Onu, A. D., Shallangwa, G. A. (2020). Kinetic and mechanism of oxidation of catechol by oxygenated [Co2(O2)(NH3)10]5+ complex. Science Frontiers, 2(1), 1-7. https://doi.org/10.11648/j.sf.20210201.11

Osunkwo, C. R., Nkole, I. U., Onu, A. D. & Idris, S. O. (2018). Electron transfer reaction of tis-(1,10-phenanthroline)cobalt(III) complex [Co(phen)3]3+ and thiosulphate ion (S2O32−) in an aqueous acidic medium. International Journal of Advance Chemistry, 6, 121-126. https://doi.org/10.14419/ijac.v6i1.11326

Osunkwo, C. R., Nkole, I. U., Onu, A. D. & Idris, S. O. (2018). Kinetics and mechanism of the reduction of tris-(1,10-phenanthroline)cobalt(III) complex by N-methylthiourea in aqueous acidic medium. Nigerian Research Journal of Chemical Sciences, 5, 82-97.

Quinones, R., Knott, H., Frost, L., Bartram, M., Clark T., Westfall T. D. & Buxo, J.A. (2024). Quantification of iron(II) in supplements using redox titration and UV-Visible spectroscopy. Journal of Chemical Education, 101(12), 5484-5491. https://doi.org/10.1021/acs.jchemed.4c01090

Rippel, R. (2012). Mercaptoacetic acid and derivatives. Ullmann's Encyclopedia Indus Chem Wiley – VCH Weinheim 40, 1626-1630.

Rodgers, G. M. & Gilreath, J. A. (2019). The Role of intravenous iron in the treatment of anemia associated with cancer and chemotherapy. Acta Haematologica, 142(1), 13-20. https://doi.org/10.1159/000496967

Sar, P. & Saha, B. (2020). Potential application of micellar nano-reactor for electron transfer reactions mediated by a variety of oxidants: aeview. Advances in Colloids and Interface Science, 284, 102241. https://doi.org/10.1016/j.cis.2020.102241

Shanmugaprabha, T., Selvakumar, K., Rajasekaran, K. & Sami, P. (2016). A kinetic study of the oxidations of 2-mercaptoethanol and 2-

mercaptoethylamine by heteropoly 11-tungsto-1-vanadophosphate in aqueous acid medium. Transition Metal Chemistry, 41, 77-85. https://doi.org/10.1007/s11243-015-9998-y

Srinivasan, B. (2022). A guide to the Michaelis-Menten equation: steady state and beyond. FEBS Journal, 289, 6086-6098. https://doi.org/10.1111/febs.16124

Ukoha, P. O., Atiga, S., Ujam, O. T., Asegbeloyin, J. N., Okpareke, O. C. & Okereke, S. O. E. (2015). Kinetics and mechanism of electron transfer reaction of an adipato bridged iron(III)-salen complex with dithionite ion in perchloric acid medium. Croatica Chemica Acta, 88, 259-266. https://doi.org/10.5562/cca2584

Umoru, P. E., Nkole, I. U. & Ezeh, T. T. (2024). Degradation of indigo carmine dye with peroxydisulphate ion in aqueous sulphuric acid phase: kinetic study. International Journal of Chemical Kinetics, 56(6), 339. https://doi.org/10.1002/kin.21710

Zhang, R., Zhao, X., He, Y., He, Y. & Ma, L. (2023). Extraction methods optimization of available heavy metals and the health risk assessment of the suburb soil in China. Environmental Monitoring and Assessments, 195(10), 1221. https://doi.org/10.1007/s10661-023-11775-9